Journal of Materials Chemistry C

ROYAL SOCIETY OF CHEMISTRY

PAPER

View Article Online
View Journal | View Issue



Cite this: J. Mater. Chem. C, 2023, 11, 3796

# Stretchable conductive nanocomposites of low electrical percolation threshold for washable high-performance-interconnects†

Seungho Kwag,‡[ab] Youngpyo Ko,‡[a] Jun-Young Jeon,‡[a] Doojoon Jang,[a] Minju Park,[a] Yoohyeon Choi,[a] Jinhan Cho [b] and Heesuk Kim *[ac]

Elastomer-based stretchable conductive composites of high electrical conductivity, mechanical stability and excellent adhesion to the substrates are essential as interconnects for stretchable electronics. Most previous composites require high percolation threshold concentration of metallic fillers to achieve high electrical conductivity, which in turn lowers their mechanical stability and adhesion to the targets. Herein, we propose a rationally designed stretchable conductive composite of low percolation threshold concentration with the aid of boron nitride (BN) as a non-conductive auxiliary filler. The BN introduction significantly increases the electrical conductivity of the composites by up to 9 orders of magnitude at 66 wt% Ag concentration. The percolation threshold Ag concentration of the composite without BNs is 63.3 wt% (14.8 vol%), whereas the introduction of 3 μm *h*-BNs lowers the threshold concentration to 52.0 wt% (9.53 vol%), which is due to the effective attractive interaction between auxiliary BN and Ag particles. Furthermore, the exfoliated 3 μm BNs lower the BN concentration to achieve similar electrical conductivity, thereby leading to improved electrical stability as well as excellent adhesion when bent or stretched. The composites have been successfully applied as stretchable electrical interconnects and maintain their performance even after repeated washings. These model studies provide an insight in that the inter-particle interaction between an auxiliary filler and a conductive filler is a key design parameter to reduce the percolation threshold concentration for high-performance stretchable conductive composites.

Received 27th October 2022,
Accepted 16th February 2023

DOI: 10.1039/d2tc04567b

rsc.li/materials-c



## Introduction

Stretchable electronics have attracted attention as promising technologies for the next generation of smart wearable devices,[1–3] personal healthcare,[4–6] and soft robotics.[7–9] A key component of stretchable electronics is a stretchable interconnect that requires high conductivity, electrical reliability upon stretching, and adhesion to flexible and/or stretchable substrates. Stretchable interconnects have been fabricated by employing inherently soft materials including liquid metals[10,11] and conductive polymers[12] or by designing stretchable structures such as wavy,[13] re-entrant,[14] chiral,[15] and serpentine structures.[16] Despite their high electrical performance, these interconnects suffer from insufficient stability against mechanical deformations, complicated process, and limited adhesion to flexible/or stretchable substrates. Furthermore, these methods require additional conductive adhesives to connect the interconnects and electronic units. Epoxy-based silver adhesives with conductivities of $10^3$–$10^5$ S cm$^{-1}$ have risen as a compelling alternative.[17–20] However, due to their limited flexibility, cracks are easily formed at the electrical interconnects and electrical components are detached from the substrates during bending or stretching, thus significantly reducing their electrical conductivity.[21] Therefore, the development of polymer-based stretchable conductive composites offering high mechanical conformability and excellent adhesion is essential for accommodating electronic islands in stretchable electronic devices.

Stretchable conductive composites have been widely explored as electrical interconnects using elastomers as a matrix and metallic materials as a conductive filler, due to their intrinsic stretchability, low sheet resistance and simple fabrication process. A variety of elastomers including polybutadiene,[22] polyurethane,[23,24] fluorinated rubber,[25] and polysilicon (*i.e.*, poly(dimethylsiloxane) (PDMS))[26,27] have been used as stretchable matrices. The electrical paths in these elastomeric matrices can be obtained by using 1, 2 or 3-dimensional shaped-metals, carbon nanotubes, MXenes, or their

[a] Soft Hybrid Materials Research Center, Korea Institute of Science and Technology (KIST), Seoul 02792, Republic of Korea. E-mail: heesukkim@kist.re.kr
[b] Chemical & Biological Engineering, Korea University, Seoul 02841, Republic of Korea
[c] Division of Energy & Environment Technology, KIST School, Korea University of Science and Technology (UST), Seoul 02792, Republic of Korea

† Electronic supplementary information (ESI) available. See DOI: https://doi.org/10.1039/d2tc04567b

‡ These authors contributed equally to this work.

mixtures.[28–31] Depending on the size, shape and type of metallic fillers, stretchable conductive composites exhibit electrical conductivity in a wide range of $10^1$–$10^5$ S cm$^{-1}$. In general, a large amount of metallic filler is required to achieve the high electrical conductivity, which increases the viscosity of the composites and in turn lowers their mechanical stability and adhesion to the targets.[26,32,33] Thus, a rational design that lowers the amount of metallic filler in an elastomeric matrix while maintaining the high electrical conductivity and good adhesion is indispensable for stretchable electronics. It should also be mentioned that, despite their importance, there have been only a few previous studies to report the adhesion of conductive interconnects to stretchable substrates.[33–36]

Here, we report a rationally designed stretchable conductive composite of high electrical conductivity and excellent adhesion to various flexible and/or stretchable substrates, which has been achieved by reducing the Ag concentration in an elastomeric matrix with the aid of boron nitride (BN) as an auxiliary filler. Due to their insulating properties, the BN fillers affect the electrical conductivity of the adhesives by tuning the effective interaction between Ag particles rather than directly participating in the electrical paths. Although only platelet-shaped *h*-BNs have been used in this study, the *h*-BN is an interesting, non-conductive auxiliary filler for model studies to investigate the shape (1, 2, and 3D) and size effect of insulating *h*-BNs on the electrical conductivity of the composites. As the diameter of *h*-BN platelets decreases from 12 to 3 μm, the electrical percolating networks of the composites can be formed at lower Ag concentrations. While the percolation threshold Ag concentration without BNs is 63.3 wt% (14.8 vol%), the introduction of 3 μm BNs lowers the threshold concentration to 52.0 wt% (9.53 vol%), with the maximum electrical conductivity of 2217 S cm$^{-1}$. This is attributed to the fact that the non-conductive 3 μm BN helps the agglomerated Ag particles better disperse in the silicone matrix compared to the larger BN particles. Furthermore, exfoliating 3 μm BNs with the aid of sucrose lowers the BN concentration to achieve similar electrical conductivity, thus resulting in improved electrical stability as well as excellent adhesion during bending or stretching.

## Experimental details

### Materials and preparation of stretchable conductive nanocomposites

Ag particles with an average size of 2–3.5 μm were purchased from Sigma-Aldrich (≥99.9% trace metal basis). Boron nitride (*h*-BN) platelets of 3, 6, and 12 μm in diameter (Fig. S1, ESI†) were purchased from 3M. Sucrose crystals were purchased from Sigma-Aldrich (≥99.5% (GC)). Introducing sucrose onto BN (sucrose-BN) was carried out using ball milling with reference to the previous study.[37] The BNs (1 g), sucrose crystals (5 g) and two $ZrO_2$ balls with a diameter of 10 mm were placed into a $ZrO_2$ pot and ball-milled at a speed of 400 rpm for 4 h. After milling, the mixture was washed with 200 mL deionized water and vacuum-filtered through a polytetrafluoroethylene (PTFE) membrane (pore size = 1.0 μm). After filtration, the sucrose-assisted BNs were dried at 80 °C for 8 h under vacuum. For composite preparation (Fig. 1(a)), the Ag particles and BNs were mixed in chloroform, followed by solvent-evaporation at 120 °C. Elastomeric silicone adhesive and 1 mL chloroform were then added to the Ag/BN mixture and mixed using a high-speed paste mixer at 2200 rpm for 3 min. The composite with a thickness of 100 μm was coated on a 1 mm thick PDMS substrate by doctor blading and cured at 180 °C for 2 h.

### Characterization

The initial sheet resistance was measured by using a standard four-point probe meter (Napson, CRESBOX) at room temperature and then the electrical resistivity was calculated by considering the initial geometry and sheet resistance of the composite films. During stretching tests, the sheet resistance was measured by a four-point probe meter (Mitsubishi Chemical Analytech, MCP-T610). Subsequently, the bulk resistivity was calculated *via* the geometrical dimension changes and sheet resistance. At a given strain, the composite thickness was obtained by measuring the width and length during stretching. It was assumed that the total volume of the composite film does not change upon stretching. The conductivity changes of the composites over 3000 stretching or bending cycles were examined when stretched or bent at a crosshead speed of 1 mm s$^{-1}$. The composite morphology was investigated using field-emission scanning electron microscopy (FE-SEM, Carl Zeiss, Sigma 300). Surface elemental analysis of the Ag and BN particles was carried out with X-ray photoelectron microscopy (XPS, PHI 5800, ESCA System) equipped with a monochromatized Al Kα radiation source. A standard adhesion test of the composites to various flexible/or stretchable substrates was conducted by attaching and detaching commercial tapes (adhesion tape, 3M).

## Results and discussion

### Effect of BN size on percolation threshold concentration

The Ag/silicone composites undergo an insulator-conductor transition as the Ag concentration increases above a critical concentration, which is called a percolation threshold concentration. The percolation theory assumes that if a bond between two Ag particles could be defined and there would be sufficiently many bonds, the percolating network would exist in the system.[38–40] For conductive composites, the bond might be defined between two Ag particles when the distance between them would be short enough for electrons to hop *via* a tunneling process.[41] The composites are non-conductive at Ag concentrations below the critical concentration, whereas the electrical percolating networks form at Ag concentrations above the critical concentration. When the Ag concentration increases above the percolation threshold concentration, the electrical conductivity of the composites increases following a scaling law equation, as shown below:[42]

$$\sigma_c = \sigma_f[(\Phi - \Phi_c)/(1 - \Phi_c)]^t$$

where $\sigma_c$ is the electrical conductivity of the composites, $\sigma_f$ is the filler conductivity, $\Phi$ is the filler volume fraction, and $\Phi_c$ is

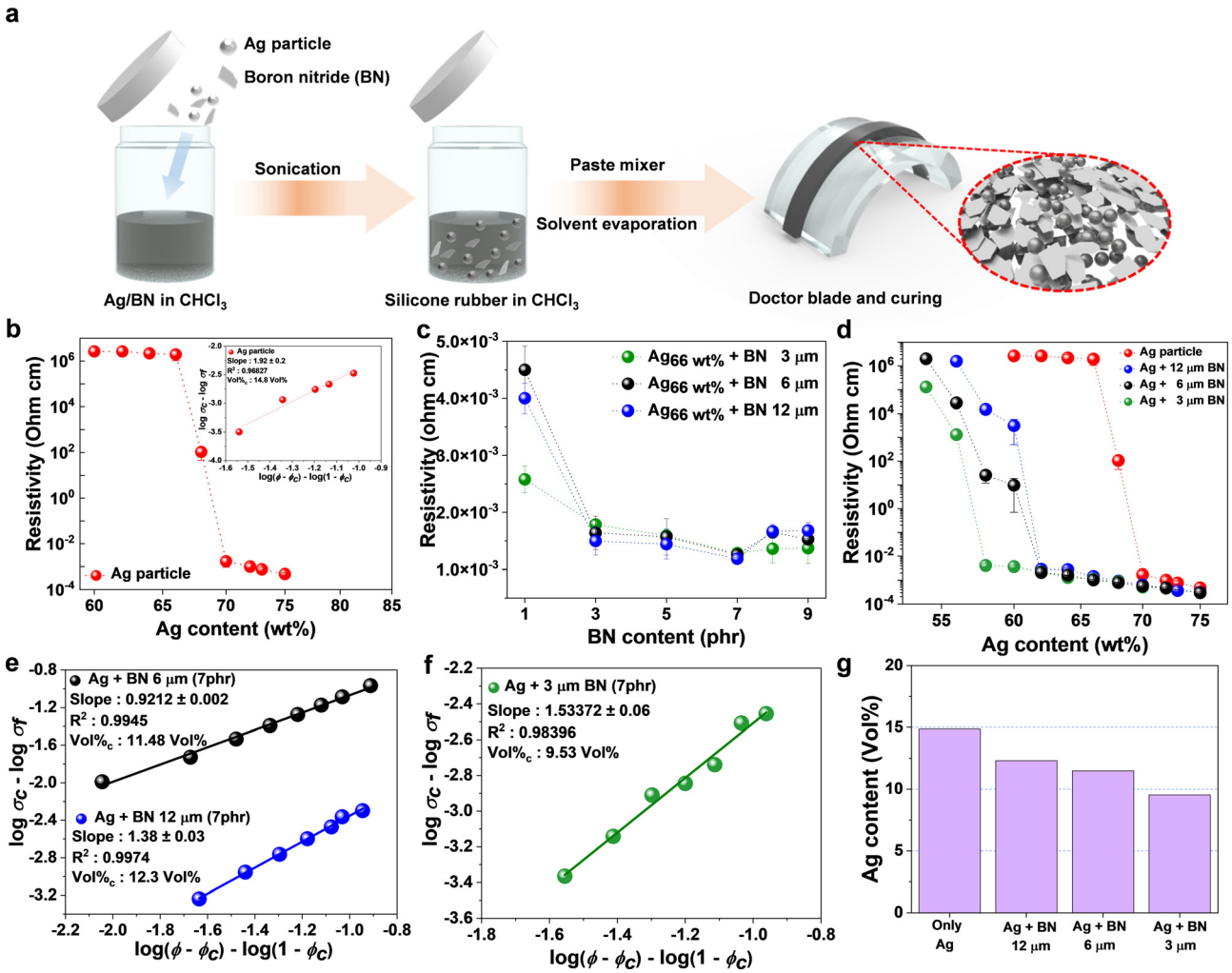


Fig. 1 (a) Preparation of the stretchable conductive adhesives. (b) Electrical resistivity of the Ag/silicone adhesives as a function of the Ag concentration. The inset is the log–log plot of $\sigma_c - \sigma_f$ *vs.* $(\Phi - \Phi_c) - (1 - \Phi_c)$ for the Ag/silicone adhesives. (c) Electrical resistivity of the Ag/silicone adhesives with *h*-BN as a function of the BN content. The Ag concentration in the composites was fixed at 66 wt%. (d) Electrical resistivity of the Ag/silicone adhesives with 7 phr *h*-BNs as a function of the Ag content. (e-f) log–log plots of $\sigma_c - \sigma_f$ *vs.* $(\Phi - \Phi_c) - (1 - \Phi_c)$ for the Ag/silicone adhesives including 7 phr BNs with various diameters (12, 6, and 3 μm). (g) Percolation threshold concentration of Ag particles in the adhesives.

the critical volume fraction. $t$ is a scaling exponent that relies on the dimensionality of the conductive network and has a theoretical value of $t = 2$ for 3-dimensional networks.[40] However, considering a quantum mechanical tunneling of electrons between two conductive particles in an insulating matrix, $t$ would be non-universal in three dimensions and varies from 1 to 3 depending on the systems.[43–45]

Fig. 1(b) shows the electrical resistivity of Ag/silicone composites as a function of the Ag concentration. When the Ag content is 66 wt% or less, the composites show the extremely high electrical resistivity of $\sim 10^6$ Ω cm. As the Ag concentration increases, the electrical resistivity decreases and reaches as low as $4.8 \times 10^{-4}$ Ω cm at 75 wt% Ag concentration. The percolation threshold concentration of the Ag particles is 63.3 wt% (14.8 vol%) and the scaling exponent ($t$) is 1.92, which are determined by a log–log plot of $\sigma_c - \sigma_f$ *vs.* $(\Phi - \Phi_c) - (1 - \Phi_c)$ (Fig. 1(b) inset). The stretchable conductive composites of Ag concentration higher than 75 wt% could not be manufactured due to their high viscosities. The high Ag content increases the composite viscosity, consequently lowering their mechanical stability and adhesion to the targets. Since the elastomeric silicone adhesive was used as a matrix, we refer to the composite as a stretchable conductive adhesive (SCA) at a later point in the manuscript.

In order to reduce the percolation threshold concentration, the platelet-shaped *h*-BNs were introduced as a non-conductive auxiliary filler to the Ag/silicone adhesives. The electrical resistivity of the $SCA_{Ag\text{-}66wt\%}$ without BN filler is $1.95 \times 10^6$ Ω cm, whereas the adhesive resistivity decreases with increasing the BN content from 1 to 7 phr (parts per hundred rubber), regardless of BN size (Fig. 1(c)). The electrical resistivity exhibits $1.19 \times 10^{-3}$, $1.26 \times 10^{-3}$, and $1.28 \times 10^{-3}$ Ω cm for the $SCA_{Ag\text{-}66wt\%}$ containing the BNs with a diameter of 12, 6, and 3 μm, respectively. However, when the BN content is higher than 7 phr, the electrical resistivity rather increases, which might be due to the unreliable film condition derived from the high viscosity. As a result, the BN introduction significantly

 

reduces the electrical resistivity of the Ag/silicone adhesives by up to 9 orders of magnitude at 66 wt% Ag concentration. The BN diameter also influences the percolation threshold concentration of the Ag particles in the adhesives (Fig. 1(d)–(g)). The percolation threshold concentration of the SCA with 12 μm BN is 58.9 wt% (12.3 vol%), which is decreased by 4.4 wt% compared to the SCA without BN filler. Reducing the BN diameter to 3 μm further lowers the percolation threshold concentration to 52.0 wt% (9.53 vol%), indicating that the smaller BN particles can effectively reduce the percolation threshold concentration.

To understand the BN effect on the percolation threshold concentration, the morphology of the SCAs was characterized by using SEM images and energy dispersive X-ray (EDX) Ag mapping (Fig. 2). At 60 wt% Ag concentration, the relatively hydrophilic Ag particles in the hydrophobic silicone matrix agglomerate due to the strong attractive interactions between Ag particles, thus deteriorating the electrical properties and exhibiting the high resistivity of $\sim 10^6$ Ω cm (Fig. 2(a) and (e)). If the attractive interaction is sufficiently strong, the Ag agglomerates may be suspended dynamically in a non-equilibrium state with a long relaxation time. Since the Ag particles form agglomerates in the SCAs, additional Ag particles are required to form the electrical percolating networks, which in turn increases the percolation threshold concentration.[35,46] In contrast, the presence of BNs in the SCAs allows the Ag particles to be better dispersed in the matrix (Fig. 2(b)–(d) and (f)–(h)). Because the BN and Ag particles have partial hydroxyl groups at their edges, they may interact attractively in the silicone matrix (Fig. S2, ESI†). Such an attractive interaction between auxiliary BN and Ag particles could compensate for the attractive interaction between Ag particles, thereby resulting in the Ag dispersion. In addition, the morphology of the Ag particles in the SCAs is subject significantly to the diameter of auxiliary BNs. As the BN diameter decreases from 12 to 3 μm, the Ag particles become dispersed even better. At the same BN concentration, smaller BNs allow more surface-BNs to interact with the Ag particles and thus prevent the agglomeration of the Ag particles, which can facilitate the Ag dispersion in the silicone matrix and in turn reduce the percolation threshold concentration of the Ag particles in the adhesives.

### Effect of exfoliated BN on the percolation threshold concentration

The optimal amount (7 phr) of BN auxiliary fillers added to the Ag/silicone adhesives occupies the high volume fraction of 2.68 vol% within the silicone matrix. Such a high content incurs a rise in the composite viscosity, which lowers the mechanical stability and adhesion to the targets. Thus, the 3 μm *h*-BN platelets were exfoliated by sucrose during planetary ball milling to lower their content in the SCAs (Fig. 3(a)).[37] The pristine *h*-BN platelets have an average thickness of 300 nm and form agglomerates (Fig. S3 and S4, ESI†). On the other hand, the sucrose-assisted *h*-BNs (suc-BNs) show an approximately 40 nm thickness and fractured structures. The size distribution analysis of suc-BN platelets also exhibits the fracture of the pristine *h*-BN platelets during the ball milling process (Fig. S5, ESI†).

The electrical resistivity of the $SCA_{Ag\text{-}66wt\%}$ was characterized as a function of the suc-BN content, exhibiting the lowest resistivity of $3.3 \times 10^{-3}$ Ω cm at 3 phr suc-BN content (Fig. 3(b)). These results indicate that the sucrose-assisted exfoliation of the pristine BNs lowers the BN amount required to achieve the percolating conductive network. However, the percolation threshold concentration of the adhesives with 3 phr suc-BNs is 61.6 wt% (13.7 vol%), which is higher than that (52.0 wt%) of the adhesives with the pristine 3 μm BNs (Fig. 3(c) and (d)). This could be due to the change in the functional groups of the pristine BNs. Owing to the grafted sucrose, the suc-BNs have more B-OR and N-R functional groups at their edges than the pristine BNs, which makes the suc-BNs relatively less hydrophilic (Fig. S6, ESI†).[37] Thermogravimetric analysis (TGA) also supports the grafting of sucrose to the BN surfaces (Fig. S7, ESI†).

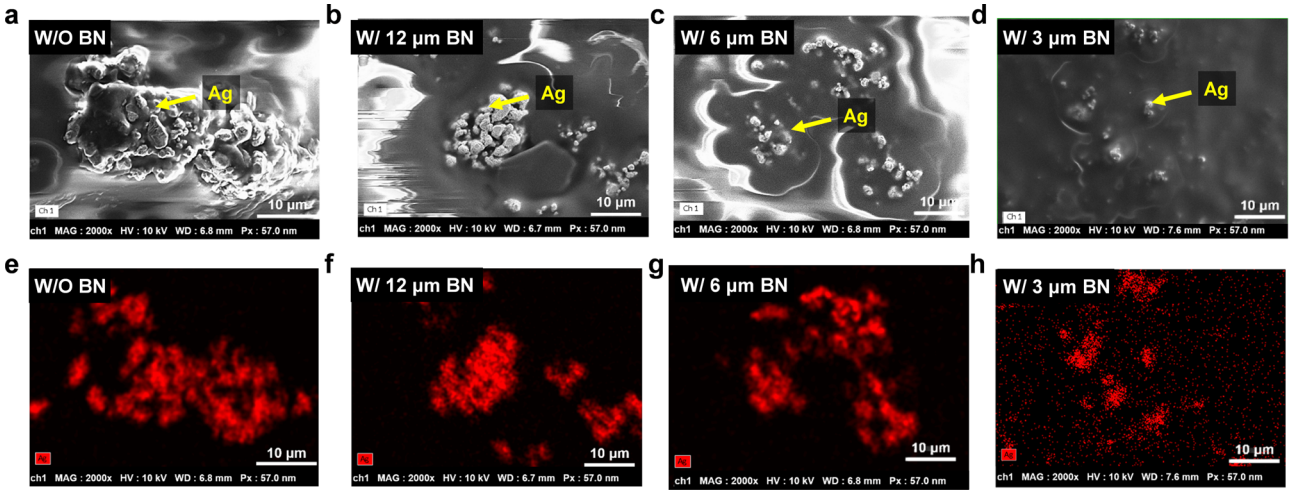


Fig. 2 SEM images and EDX Ag mapping of the Ag/silicone adhesives with 60 wt% Ag content: (a and e) No BN platelets in the adhesive, (b and f) 12 μm BNs, (c and g) 6 μm BNs, and (d and h) 3 μm BNs. All scale bars indicate 10 μm.

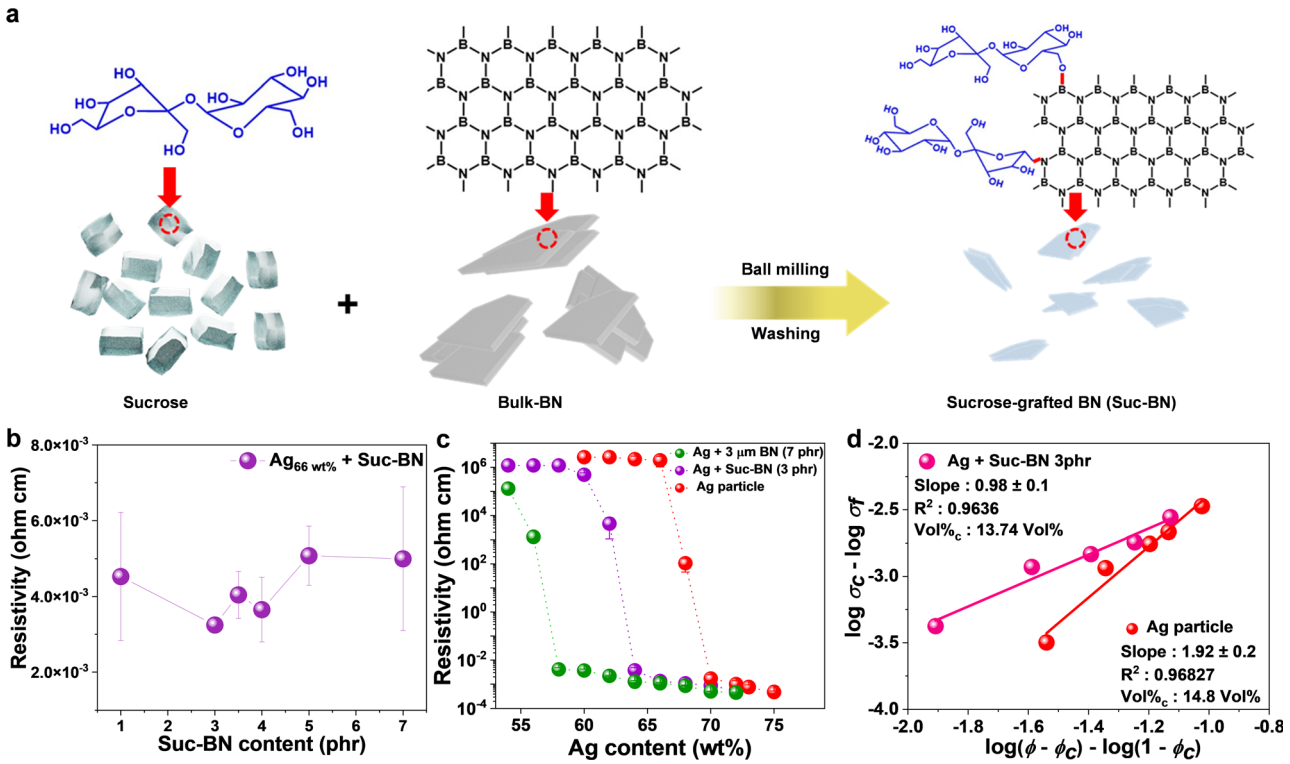


Fig. 3 (a) Sucrose-assisted exfoliation of the pristine 3 μm BNs. (b) Electrical resistivity of the Ag/silicone adhesives with suc-BN as a function of the suc-BN content. The Ag concentration in the composites was fixed at 66 wt%. (c) Electrical resistivity of the Ag/silicone adhesives with 3 phr suc-BNs as a function of the Ag content. (d) log–log plots of $\sigma_c - \sigma_f$ *vs.* $(\Phi - \Phi_c) - (1 - \Phi_c)$ for the Ag/silicone adhesives without BNs and with 3 phr suc-BNs.

The weak attractive interaction between the relatively hydrophobic suc-BN and the hydrophilic Ag particle could not prevent some agglomeration of the Ag particles, which is consistent with the SEM images and EDX Ag mapping as shown in Fig. S8 (ESI†). As a result, the poor dispersion of Ag particles in the adhesives with 3 phr suc-BNs leads to an increase in the percolation threshold concentration compared to the adhesives with the pristine 3 μm BNs of 7 phr. In order to reduce the BN amount without deteriorating the Ag dispersion, the studies of exfoliating the BN platelets *via* a hydrophilic surfactant have been in progress.

### Electrical stability of the adhesives under strain

The SCA films with a thickness of 100 μm were printed on a 1 mm thick PDMS substrate by doctor blading. The SCAs containing only the 72 wt% ($SCA_{Ag\text{-}72\ wt\%}$) and 73 wt% ($SCA_{Ag\text{-}73\ wt\%}$) Ag particles show the electrical conductivity of 1420 and 1755 S $cm^{-1}$, respectively. In contrast, the SCAs containing the 72 wt% Ag particles and 7 phr BNs show the higher conductivity of 1959, 2048 and 2213 S $cm^{-1}$ for BN diameters of 12, 6, and 3 μm, respectively, due to the good dispersion of Ag particles as explained above. When stretched up to 90% under uniaxial tensile stress, the $SCA_{Ag\text{-}72\ wt\%}$ and $SCA_{Ag\text{-}73\ wt\%}$ exhibit similar conductivity changes ($\sigma/\sigma_0$, where $\sigma$ and $\sigma_0$ are the changed and initial conductivity, respectively) of 0.39 and 0.4, respectively (Fig. 4(a)). However, the SCAs with 7 phr BNs exhibit a slightly higher reduction in the conductivity upon stretching; the conductivity changes ($\sigma/\sigma_0$) for 3, 6, and 12 μm BNs are 0.33, 0.27, and 0.33, respectively, which might be attributed to the fact that the large amount of 7 phr BNs significantly reduces the volume fraction of the silicone matrix in the composites and thus increases the SCA viscosity. Reducing the BN concentration required to lower the percolation threshold Ag concentration is effective in controlling the adhesive viscosity along with stretchable stability. As shown in Fig. 4(b), the initial conductivity of the $SCA_{Ag\text{-}72wt\%}$ with suc-BN is 1965 S $cm^{-1}$ and its conductivity change is 0.46 at 90% strain, which is an improved electrical stability compared to the SCAs without BNs or with un-exfoliated BNs. Such an electrical stability is also confirmed in the stretching at 50% strain and bending tests with a bending radius of 10 mm over 3000 cycles (Fig. 4(c) and (d)). For $SCA_{Ag\text{-}72wt\%}$ without BNs, the $\sigma/\sigma_0$ are 0.13 and 0.67 after 3000 stretching and bending cycles, respectively. The $SCA_{Ag\text{-}72wt\%}$ with 7 phr 3 μm BNs shows the same instability as the adhesive without BNs, whereas the $SCA_{Ag\text{-}72wt\%}$ with 3 phr suc-BNs exhibits significantly higher electrical stabilities of $\sigma/\sigma_0 = 0.53$ and 0.83 for stretching and bending cycles, respectively. These results demonstrate that reducing the BN concentration is essential to maintain the high volume fraction of the silicone matrix in the composites for stretchable stability and good adhesion. In addition, this work was compared to recent works on conductive elastomers and conductive adhesives (Fig. S9, ESI†). Since few studies on elastomer-based conductive adhesives have been reported, the electrical conductivities of the SCAs as a function of uniaxial tensile strain are compared with the recent works on elastomer-based conductive composites. Fig. S9 (ESI†) shows that the electrical conductivity and stability under strain of the SCA are among the high results of previous studies.

 

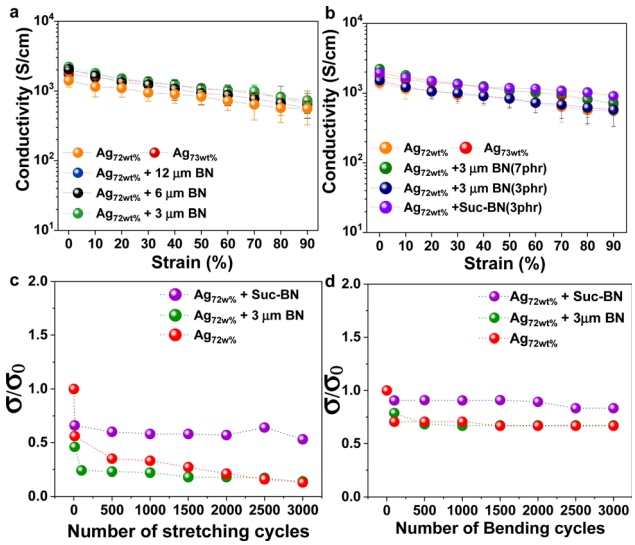


Fig. 4 (a, b) Electrical conductivity of the Ag/silicone adhesives as a function of the strain. Change in conductivity ($\sigma/\sigma_0$, where $\sigma$ and $\sigma_0$ are the changed and initial conductivity, respectively) of the Ag/silicone adhesives as a function of (c) number of bending cycles at a bending radius of 10 mm and (d) number of stretching cycles at 50% strain.

## Adhesion of the adhesives to flexible and/or stretchable substrates

While conventional epoxy-based Ag adhesives have higher electrical conductivity than our SCA, they have some disadvantages of rigidity and poor adhesion to various flexible and/or stretchable substrates. Due to their limited flexibility, cracks are easily formed at the electrical interconnects and electrical components are detached from the substrates when bent or stretched, thereby significantly reducing their electrical conductivity (Fig. S10, ESI†). Although the stretchable substrates such as PDMS have been widely used for wearable devices, a few studies have been reported to date.[47–50] We conducted the standard adhesion tests of the SCAs with 3 phr suc-BN on various flexible and/or stretchable substrates such as PDMS, PI (polyimide), PES (polyethersulfone), and PEN (polyethylene naphthalate). While the epoxy-based conductive adhesives (ECA) are removed from PDMS, PI and PES by the standard adhesion tests, none of the SCAs with suc-BN are detached from the substrates (Fig. 5(a)–(d)). Moreover, the SCAs are strongly attached on the PDMS, PI, PES and PEN substrates even after bending, indicating that the addition of suc-BNs as an auxiliary filler does not affect the adhesion properties of silicone adhesives used as a matrix (Fig. 5(e)–(h)).

## Demonstration of the adhesives as washable electrical interconnects

The SCAs in this study meet the requirements for stretchable/or wearable interconnects such as high electrical conductivity, stability against strain, and adhesion to various substrates. Attached to a human finger-joint, the SCA printed on a PDMS substrate successfully interconnects between a battery and an electrical propeller without additional soldering or commercial epoxy-based conductive adhesives (Fig. 6(a)–(c)). The spin speed of the propeller connected to the SCA remains constant regardless of the bending angle of a human finger-joint, which is also confirmed by the paper position. Furthermore, as shown in Fig. 6(d)–(f), the SCA interconnecting between a battery and a red light-emitting diode (LED) works reliably regardless of the bending motion. It is worth mentioning that the SCA interconnects

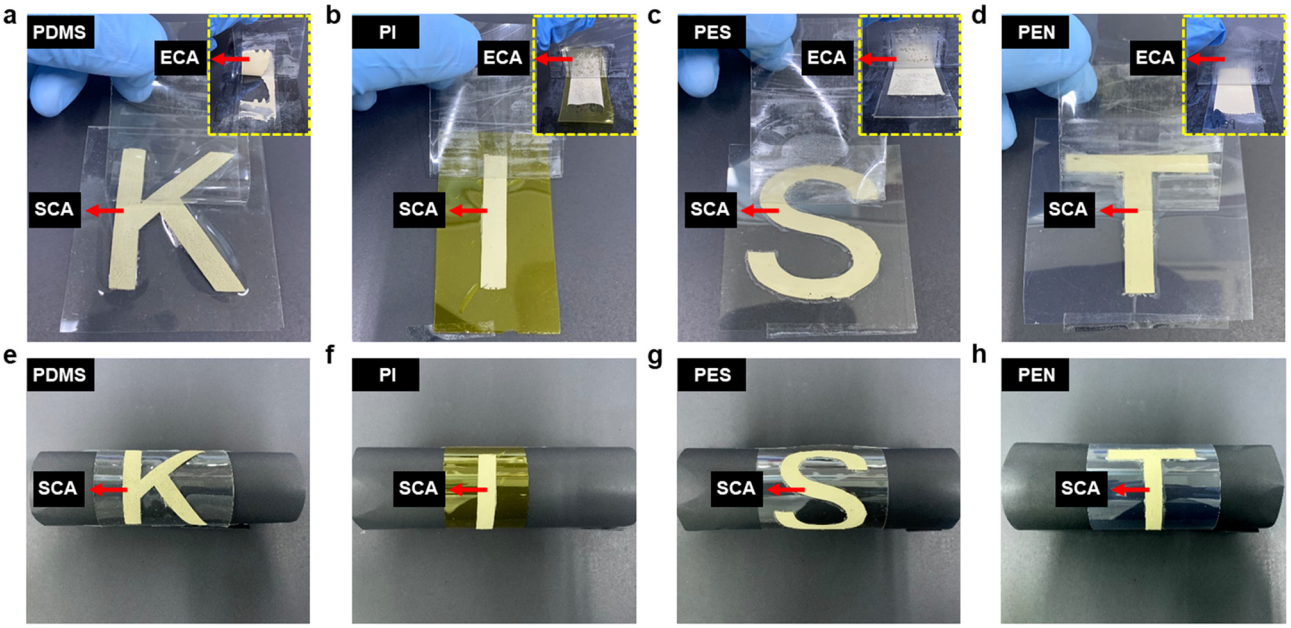


Fig. 5 Adhesion of the SCAs containing the 72 wt% Ag particles and 3 phr suc-BNs to various substrates: (a and e) PDMS, (b and f) PI, (c and g) PES, and (d and h) PEN. The insets show the adhesion of commercial epoxy-based conductive adhesives (electrically conductive adhesives (ECA)) to the indicated substrates.

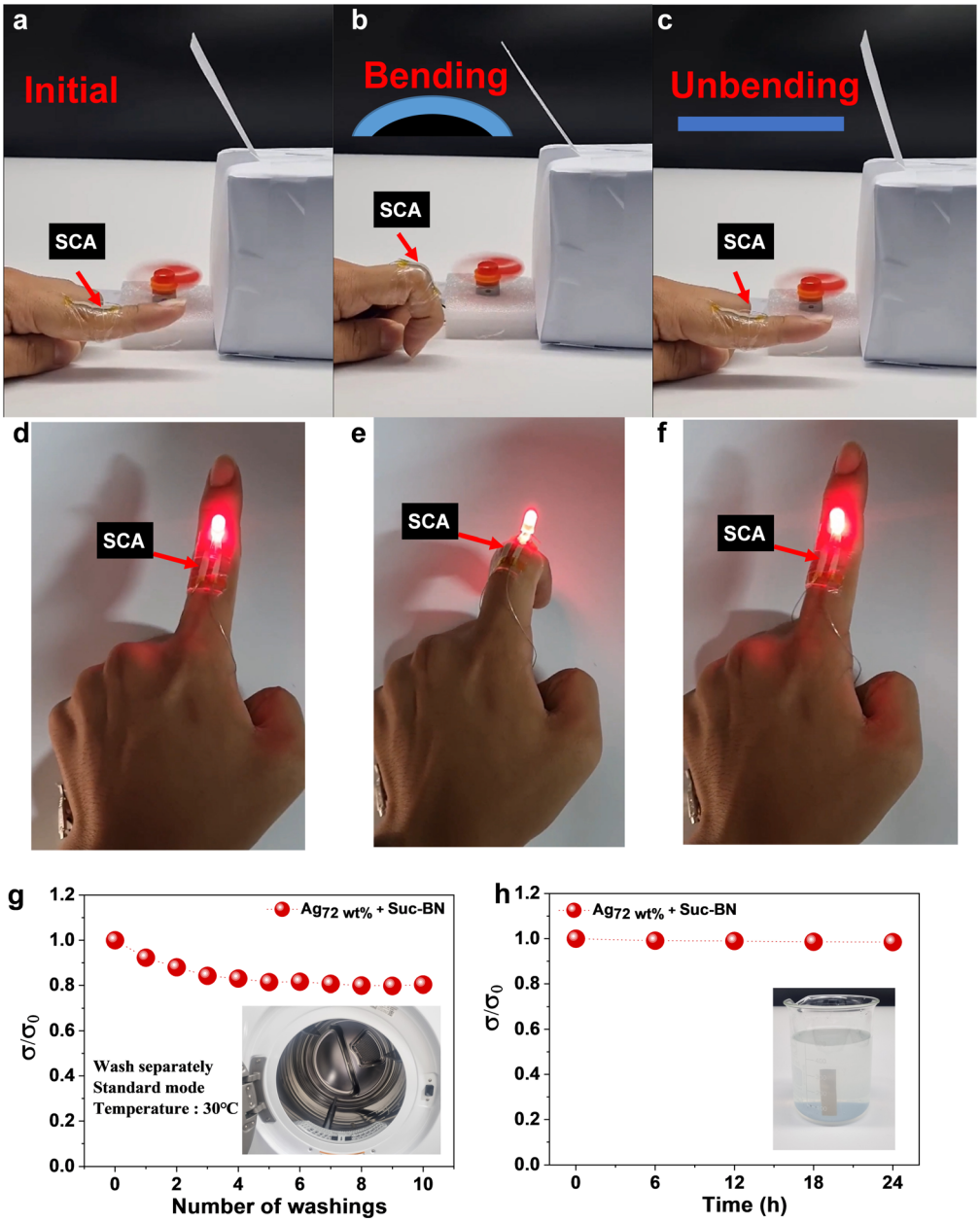


Fig. 6 Demonstration of the stretchable conductive adhesives as electrical interconnects. Performance of the SCAs interconnecting a battery with an electrical propeller (or a LED) on a human finger-joint under (a and d) initial state, (b and e) bending state, and (c and f) unbending state. Change in the electrical conductivity of the SCA interconnects on PDMS (g) after being immersed in 1 wt% detergent solution for 24 h and (h) after 10 repeated washings using a conventional washing machine in standard mode.

maintain their electrical conductivity after being immersed in 1 wt% detergent solution for 24 h (Fig. 6(g)). Even after 10 repeated washings using a household washing machine with detergent solution at 30 °C in standard mode, the SCA performance remains about 80% (Fig. 6(h)), indicating their great potential as stretchable interconnects, especially washable textile interconnects.

## Conclusions

A rationally designed stretchable conductive adhesive (SCA) of high electrical conductivity and excellent adhesion has been achieved by reducing the Ag concentration with the aid of boron nitride (BN) as a non-conductive auxiliary filler in the composites. Due to their insulating properties, the BN fillers influence the electrical conductivity of the composites by controlling the effective attractive interaction between Ag particles rather than directly participating in the electrical paths. The BN introduction significantly increases the electrical conductivity of the $SCA_{Ag\text{-}66wt\%}$ by up to 9 orders of magnitude. With decreasing the diameter of *h*-BN platelets from 12 to 3 μm, the electrical percolating networks of the adhesives are formed at lower Ag concentrations. The percolation threshold Ag

 

concentration of the SCA without BNs is 63.3 wt% (14.8 vol%), whereas the introduction of 3 μm BNs lowers the threshold concentration to 52.0 wt% (9.53 vol%), with the maximum electrical conductivity of 2217 S $cm^{-1}$, which is due to the effective attractive interaction between auxiliary BN and Ag particles. Such an interaction could compensate for the attractive interaction between Ag particles, thereby resulting in the enhanced Ag dispersion. In contrast, the exfoliated 3 μm BNs assisted by sucrose are less effective in reducing the percolation threshold concentration than the pristine 3 μm BNs, owing to their less hydrophilic surface. Nevertheless, the exfoliated 3 μm BNs lower the BN concentration to achieve similar electrical conductivity, thus resulting in improved electrical stability as well as excellent adhesion when bent or stretched. These results demonstrate that the inter-particle interaction between an auxiliary filler and a conductive filler is a key design parameter to reduce the percolation threshold concentration for mechanical and electrical stability of the stretchable conductive composites. Attached to a human finger-joint, the SCAs have been successfully applied as electrical interconnects between a battery and a propeller (or LED) without additional soldering or commercial conductive adhesives. In addition, the SCAs maintain their performance even after repeated washings using a conventional washing machine in standard mode. We believe that the strategy proposed in this study shows great potential for stretchable electronics, especially washable textile electronics.

## Author contributions

Seungho Kwag, Youngpyo Ko and Jun-Young Jeon: investigation, data acquisition, and writing the original draft. Doojoon Jang, Minju Park and Yoohyeon Choi: data analysis and visualization. Jinhan Cho: conceptualization and supervision. Heesuk Kim: project administration, supervision, funding acquisition, and writing-review & editing.

## Conflicts of interest

The authors have no conflicts to declare.

## Acknowledgements

This research was supported by the Korea Institute of Science and Technology (KIST) Future Resource Research Program (2E31161), the National Research Foundation of Korea (NRF-2019R1A2C2091094), and the Creative Materials Discovery Program through the NRF grant funded by the Ministry of Science and ICT (2020M3D1A1110499). This work was also supported by National R&D Program though the NRF funded by the Ministry of Science and ICT (2020M3D1A2101799).

## References

1 M. Hu, Y. Gao, Y. Jiang, H. Zeng, S. Zeng, M. Zhu, G. Xu and L. Sun, *Adv. Compos. Hybrid Mater.*, 2021, **4**, 514–520.
2 D. Son, J. Lee, S. Qiao, R. Ghaffari, J. Kim, J. E. Lee, C. Song, S. J. Kim, D. J. Lee, S. W. Jun, S. Yang, M. Park, J. Shin, K. Do, M. Lee, K. Kang, C. S. Hwang, N. Lu, T. Hyeon and D. H. Kim, *Nat. Nanotechnol.*, 2014, **9**, 397–404.
3 M. Gao, L. Li and Y. Song, *J. Mater. Chem. C*, 2017, **5**, 2971–2993.
4 M. D. Bartlett, E. J. Markvicka and C. Majidi, *Adv. Funct. Mater.*, 2016, **26**, 8496–8504.
5 T. Dinh, H.-P. Phan, T.-K. Nguyen, A. Qamar, A. R. M. Foisal, T. N. Viet, C.-D. Tran, Y. Zhu, N.-T. Nguyen and D. V. Dao, *J. Mater. Chem. C*, 2016, **4**, 10061–10068.
6 P. A. Lopes, H. Paisana, A. T. De Almeida, C. Majidi and M. Tavakoli, *ACS Appl. Mater. Interfaces*, 2018, **10**, 38760–38768.
7 J. Z. Gul, M. Sajid, M. M. Rehman, G. U. Siddiqui, I. Shah, K. H. Kim, J. W. Lee and K. H. Choi, *Sci. Technol. Adv. Mater.*, 2018, **19**, 243–262.
8 N. Lu and D. H. Kim, *Soft Robot.*, 2014, **1**, 53–62.
9 Y. Chen, X. Zhao, Z.-Y. Jon, Y. Yang, M.-B. Yang and B. Yin, *J. Mater. Chem. C*, 2021, **9**, 5515–5527.
10 H. Hwang, M. Kong, K. Kim, D. Park, S. Lee, S. Park, H.-J. Song and U. Jeong, *Sci. Adv.*, 2021, **7**, eabh0171.
11 E. J. Markvicka, M. D. Bartlett, X. Huang and C. Majidi, *Nat. Mater.*, 2018, **17**, 618–624.
12 I. You, M. Kong and U. Jeong, *Acc. Chem. Res.*, 2019, **52**(1), 63–72.
13 D. Qi, Z. Liu., Y. Liu, W. R. Leow, B. Zhu, H. Yang, J. Yu, W. Wang, H. Wang, S. Yin and X. Chen, *Adv. Mater.*, 2015, **27**, 5559–5566.
14 S. Kang, T. H. Kang, B. S. Kim, J. Oh, S. Park, I. S. Choi, J. Lee and J. G. Son, *Composites, Part B*, 2019, **162**, 580–588.
15 L. Zhou, Y. Peng, Y. Wang, M. Lu, J. Zhou, J. Ding and T. Sang, *J. Opt. Soc. Am. B*, 2020, **37**, 3763–3768.
16 D. Kong, Z. M. El-Bahy, H. Algadi, T. Li, S. M. El-Bahy, M. A. Nassan, J. Li, A. A. Faheim, A. Li, C. Xu, M. Huang, D. Cui and H. Wei, *Adv. Compos. Hybrid Mater.*, 2022, 1–12.
17 M. Zulkarnain, M. A. Fadzil, M. Mariatti and I. A. Azid, *J. Electron. Mater.*, 2017, **46**, 6727–6735.
18 C. Li, Q. Li, X. Long, T. Li, J. Zhao, K. Zhang, E. Songfeng, J. Zhang, Z. Li and Y. Yao, *ACS Appl. Mater. Interfaces*, 2017, **9**, 29047–29054.
19 S. Nam, H. W. Cho, T. Kim, D. Kim, B. J. Sung, S. Lim and H. Kim, *Appl. Phys. Lett.*, 2011, **99**, 2–4.
20 H. Wu, S. Chiang, W. Han, Y. Tang, F. Kang and C. Yang, *Compos. Sci. Technol.*, 2014, **99**, 109–116.
21 R. Ma, S. Kwon, Q. Zheng, H. Y. Kwon, J. Il. Kim, H. R. Choi and S. Baik, *Adv. Mater.*, 2012, **24**, 3344–3349.
22 S. Ata, T. Mizuno, A. Nishizawa, C. Subramaniam, D. N. Futaba and K. Hata, *Sci. Rep.*, 2014, **4**, 1–8.
23 S. Shang, W. Zeng and X. M. Tao, *J. Mater. Chem.*, 2011, **21**, 7274–7280.
24 H. J. Hong, S. M. Kwan, D. S. Lee, S. M. Kim, Y. H. Kim, J. S. Lim, J. Y. Hwang and H. S. Jeong, *Compos. Sci. Technol.*, 2017, **152**, 94–100.
25 N. Matsuhisa, D. Inoue, P. Zalar, H. Jin, Y. Matsuba, A. Itoh, T. Yokota, D. Hashizume and T. Someya, *Nat. Mater.*, 2017, **16**, 834–840.

26 A. Larmagnac, S. Eggenberger, H. Janossy and J. Vörös, *Sci. Rep.*, 2014, **4**, 1–7.
27 S. Stassi and G. Canavese, *J. Polym. Sci., Part B: Polym. Phys.*, 2012, **50**, 984–992.
28 K. Ke, Z. Sang and I. Manas-Zloczower, *Nanoscale Adv.*, 2019, **1**, 2337–2347.
29 Z. Sang, K. Ke and I. Manas-Zloczower, *ACS Appl. Polym. Mater.*, 2019, **1**, 714–721.
30 Y. Li, Y. Chen, J.-D. Gu, K. Ke, B. Yin and M.-B. Yang, *J. Mater. Chem. B*, 2021, **42**, 8801–8808.
31 Y. Li, S. Wang, Z. C. Xiao, Y. Yang, B. W. Deng, B. Yin, K. Ke and M. B. Yang, *J. Mater. Chem. C*, 2020, **8**, 4040–4048.
32 Y. Kim, J. Zhu, B. Yeom, M. Di Prima, X. Su, J. G. Kim, S. J. Yoo, C. Uher and N. A. Kotov, *Nature*, 2013, **500**, 59–63.
33 J. Hao, D. Wang, S. Li, X. He, J. Zhou and F. Xue, 18th Int. Conf. Electron. Packag. Technol. ICEPT 2017, 2017, pp. 803–808.
34 J. Luo, Z. Cheng, C. Li, L. Wang, C. Yu, Y. Zhao, M. Chen, Q. Li and Y. Yao, *Compos. Sci. Technol.*, 2016, **129**, 191–197.
35 Y. Ko, J. Oh, K. T. Park, S. Kim, W. Huh, B. J. Sung, J. A. Lim, S. S. Lee and H. Kim, *ACS Appl. Mater. Interfaces*, 2019, **11**, 37043–37050.
36 J. Dou, L. Tang, L. Mou, R. Zhang and X. Jiang, *Compos. Sci. Technol.*, 2020, **197**, 108237.
37 S. Chen, R. Xu, J. Liu, X. Zou, L. Qiu, F. Kang, B. Liu and H. M. Cheng, *Adv. Mater.*, 2019, **31**, 1–10.
38 J. Li and J. K. Kim, *Compos. Sci. Technol.*, 2007, **67**, 2114–2120.
39 C. W. Nan, Y. Shen and J. Ma, *Annu. Rev. Mater. Res.*, 2010, **40**, 131–151.
40 D. Stauffer, A. Aharony and S. Redner, *Phys. Today*, 1993, **46**, 64.
41 P. Gonon and A. Boudefel, *J. Appl. Phys.*, 2006, **99**, 024308.
42 S. Stankovich, D. A. Dikin, G. H. B. Dommett, K. M. Kohlhaas, E. J. Zimney, E. A. Stach, R. D. Piner, S. B. T. Nguyen and R. S. Ruoff, *Nature*, 2006, **442**, 282–286.
43 A. Celzard and J. F. Marêché, *Phys. A*, 2003, **317**, 305–312.
44 D. S. McLachlan, C. Chiteme, C. Park, K. E. Wise, S. E. Lowther, P. T. Lillehei, E. J. Siochi and J. S. Harrison, *J. Polym. Sci., Part B: Polym. Phys.*, 2005, **43**, 3273–3287.
45 J. W. Essam, *Reports Prog. Phys.*, 1980, **43**, 833–912.
46 H. W. Cho, S. Nam, S. Lim, D. Kim, H. Kim and B. J. Sung, *J. Appl. Phys.*, 2014, **115**, 154307.
47 S. Q. Wang, T. Chinnasamy, M. A. Lifson, F. Inci and U. Demirci, *Trends Biotechnol.*, 2016, **34**, 909–921.
48 J. H. Moon, D. H. Baek, Y. Y. Choi, K. H. Lee, H. C. Kim and S. H. Lee, *J. Micromech. Microeng.*, 2010, **20**, 025032.
49 J. Chen, J. Zheng, Q. Gao, J. Zhang, J. Zhang, O. M. Omisore, L. Wang and H. Li, *Appl. Sci.*, 2018, **8**, 345.
50 D. Qi, K. Zhang, G. Tian, B. Jiang and Y. Huang, *Adv. Mater.*, 2021, **33**, 1–25.

 